Int. J. Heat Mass Transfer. Vol. 19, pp. 1257–1266. Pergamon Press 1976. Printed in Great Britain

FREE CONVECTION HEAT TRANSFER FROM ISOTHERMAL SPHERES IN POLYMER SOLUTIONS

WAYNE S. AMATO and CHI TIEN
Department of Chemical Engineering and Materials Science, Syracuse University, Syracuse, NY 13210, U.S.A.

(*Received* 12 *February* 1974 *and in revised form* 12 *February* 1976)

Abstract—An experimental investigation of natural convection heat transfer from isothermal spheres to aqueous polymer solutions is reported. The power law model was used to correlate the data according to the theory of Acrivos [2]. Temperature profiles have been measured about an isothermal sphere in various polymer solutions and hot-film anemometry has been used to measure velocity profiles about a sphere in free convection heat transfer in a polymer solution. Quantitative information on the boundary-layer thicknesses was also obtained.

NOMENCLATURE

C_p, specific heat per unit mass [J/kg K];
D, diameter [m];
$f(\eta)$, velocity similarity variable;
g, gravitational acceleration [m/s^2];
Gr, generalized Grashof number, $= \dfrac{\rho^2 R^{n+2}(\beta g \Delta T)^{2-n}}{K^2}$;
h, heat-transfer coefficient, $= q/\Delta T$;
k, thermal conductivity [J/m·s K];
K, fluid consistency index for power law fluid [N·s^n/m^2];
n, flow parameter index for power law fluid;
$\bar{N}u$, average Nusselt number, $= hR/k$;
Pr, generalized Prandtl number–Power law fluid, $= (\rho C_p/k)(K/\rho)^{2/(1+n)} R^{(1-n)/(1+n)} \times [Rg\beta\Delta T]^{[3(n-1)]/[2(1+n)]}$;
q, heat flux [J/m^2 s];
R, radius of spheres [m], or resistance [Ω];
r_i, r/R where r is the distance of a point on the surface of a sphere from the axis of symmetry;
T, temperature [K];
T_w, wall temperature [K];
T_∞, bulk temperature [K];
ΔT, $T_w - T_\infty$;
u, velocity component along the x-direction;
u_1, dimensionless velocity, $= u/\sqrt{(Rg\beta\Delta T)}$;
u_2, dimensionless scaled velocity, $= u_1(Pr)^{(n+1)/(3n+1)}$;
$\bar{u}_2$, u_2/r_1;
v, velocity component along y-direction;
v_1, dimensionless velocity, $= vGr^{[2(n+1)]^{-1}}/\sqrt{(Rg\beta\Delta T)}$;
v_2, dimensionless scaled velocity in y-direction, $= \dfrac{v_1}{(Pr)^{(2n+1)/(3n+1)}}$;
x, distance along surface from stagnation point [m];
x_1, $\dfrac{x}{R}$, dimensionless distance;
X, $= \int_0^{x_1} r_1(x_1)\,dx_1$;
y, distance normal to surface [m];
y_1, dimensionless normal distance, $= \dfrac{y(Gr)^{1/[2(n+1)]}}{R}$;
y_2, scaled dimensionless y-distance, $= y_1/(Pr)^{n/(3n+1)}$.

Greek symbols

α, thermal diffusivity or temperature coefficient of resistance;
β, coefficient of thermal expansion of fluid [K];
γ, shear rate [s^{-1}];
δ_T, thermal boundary-layer thickness;
δ_v, velocity boundary-layer thickness;
ε, angle between normal to the surface and the direction of the body force vector;
η, dimensionless similarity variable;
θ, dimensionless temperature, $= (T - T_\infty)/(T_w - T_\infty)$;
ρ, fluid density [kg/m^3];
τ_{xy}, x–y component of stress tensor;
ϕ, angular position from stagnation point.

INTRODUCTION

THEORETICAL and experimental investigations of a natural convection heat transfer from spheres have been few. In a previous paper [1], the results for free convection heat transfer in water from isothermal spheres was reported. There appears to be no experimental measurements of heat transfer from spheres operating in free convection in non-Newtonian polymer solutions.

The only comprehensive treatment of free convection about a sphere with a power law rheological formulation, has been given in the outstanding paper by Acrivos [2].

The objectives of this study are to correlate experimentally the free convective heat transfer around a

sphere immersed in widely differing non-Newtonian polymer solutions and to measure the temperature and velocity profiles around a sphere operating in free convection in a polymer solution.

Theory

Acrivos' theory [2] is unique since it describes natural convection heat transfer from two-dimensional and axisymmetric bodies to Newtonian and power law non-Newtonian fluids. The theory is developed, first with reference to the two-dimensional case and later extended to the three-dimensional axisymmetric case through the use of a Mangler-type transformation.

The equations describing axisymmetric heat transfer by natural convection in a power law fluid are:

$$\frac{\partial(ru)}{\partial x}+\frac{\partial(rv)}{\partial y}=0 \tag{1}$$

$$u\frac{\partial u}{\partial x}+v\frac{\partial u}{\partial y}=g\beta\Delta T\theta\sin\varepsilon+\frac{K}{\rho}\frac{\partial}{\partial y}\left[\frac{\partial u}{\partial y}\left|\frac{\partial u}{\partial y}\right|^{n-1}\right] \tag{2}$$

$$u\frac{\partial\theta}{\partial x}+v\frac{\partial\theta}{\partial y}=\alpha\frac{\partial^2\theta}{\partial y^2} \tag{3}$$

where

$$\rho_\infty/\rho=1+\beta(T-T_\infty) \tag{4}$$

and r is the distance (normal) from the axis of symmetry to a point on the surface.

The boundary conditions are:

$$\begin{aligned} &y=0;\quad u=0,\quad v=0,\quad \theta=1\\ &y=\infty \text{ and } x=0;\quad u=0,\quad \theta=0. \end{aligned} \tag{5}$$

In equation (2), the two-dimensional form of the power law is employed, viz.,

$$\tau_{xy}=K\left|\frac{\partial u}{\partial y}\right|^{n-1}\frac{\partial u}{\partial y}. \tag{6}$$

Using the Mangler-type transformation:

$$r_1=\frac{r(x_1)}{R};\quad \bar{u}_2=u_2r_1;\quad X=\int_0^{x_1}r_1(x_1)\,dx_1. \tag{7}$$

Equations (1), (2) and (3) become:

$$\frac{\partial\bar{u}_2}{\partial X}+\frac{\partial v_2}{\partial y_2}=0 \tag{8}$$

$$0=r_1\theta\sin\varepsilon+\frac{\partial^2\bar{u}_2}{\partial y_2} \tag{9}$$

$$\bar{u}_2\frac{\partial\theta}{\partial X}+v_2\frac{\partial\theta}{\partial y_2}=\frac{\partial^2\theta}{\partial y_2^2}. \tag{10}$$

The above equations (8)–(10) can be transformed to ordinary differential equations by defining (for a sphere $r_1=\sin x_1$ and $\sin\varepsilon=\sin x_1$).

$$\bar{u}_2=(\sin x_1)^{1/n}\left[\left[\frac{3n+1}{2n+1}\left[\frac{1}{(\sin x_1)^2}\right]^{(3n+1)/[n(2n+1)]}\right]\times\left[\int_0^{x_1}(\sin x_1)^{(2n+3)/(2n+1)}\,dx_1\right]\right]^{n/(3n+1)}f'(\eta) \tag{11}$$

$$\theta=\theta(\eta) \tag{12}$$

where

$$\eta=\frac{y_2}{\left[\frac{3n+1}{2n+1}\left[\frac{1}{(\sin x_1)^2}\right]^{(3n+1)/[n(2n+1)]}\int_0^{x_1}(\sin x_1)^{(2n+3)/(2n+1)}\,dx_1\right]^{n/(3n+1)}}. \tag{13}$$

The ordinary differential equations obtained are:

$$\frac{d}{d\eta}(f'')^n+\theta=0 \tag{14}$$

$$\theta''+f\theta'=0 \tag{15}$$

subject to

$$\theta(0)=1,\ \theta(\infty)=0,\ f(0)=f'(0)=f''(\infty)=0. \tag{16}$$

Acrivos solved equations (14) and (15) around $\eta=0$, since this is necessary for evaluation of the heat-transfer coefficient. The general form for the average Nusselt numbers is:

$$\overline{Nu}=CGr^{1/[2(n+1)]}Pr^{n/(3n+1)} \tag{17}$$

where C is dependent on n (weakly) and (17) is valid for

$$Pr>10 \tag{18}$$

and

$$Gr^{1/[2(n+1)]}Pr^{n/(3n+1)}>10. \tag{19}$$

Hot-film anemometry work in non-Newtonian fluids is very scarce. Therefore no attempt will be made to discuss theoretical estimation methods in the measurement of velocity profiles. Direct calibration has been used and this will be discussed in the experimental section.

EXPERIMENTAL EQUIPMENT

The experimental equipment consisted of the following: (a) copper spheres with internal heating elements, (b) heat-transfer tank, (c) power supply and power measuring equipment, (d) traversing mechanism for holding and positioning velocity or temperature probes, (e) thermocouple probe, (f) hot-film anemometry calibration and measuring equipment, (g) physical property measuring equipment for density, thermal conductivity, and rheological properties.

Four sphere sizes were used in the experimental investigations. They had nominal diameters of 0.0254, 0.0508, 0.0762 and 0.1016 m. They were heated electrically and were composed of a nichrome winding on a ceramic core surrounded by tightly-fitting hemispherical copper shells. Five copper–constantan thermocouples of 40 B and S gauge wire were internally embedded into the copper shell to enable wall temperature measurement. They were calibrated beforehand using two fixed points—ice and steam with a quadratic in e.m.f. vs T. See [1] and [3] for more detailed descriptions.

Each sphere was suspended in a 0.2839 m^3 plexiglas tank from its support tube. The tank dimensions were $0.762\times0.508\times0.762$ m.

The power supply for the heating elements utilized 110V A.C. which was regulated to 0.1% by a voltage regulator and could be continuously varied by using autotransformers. Power to the spheres was measured by three precision wattmeters capable of 0.25% accuracy over a range of several watts to 1000W. Provision

was also made to accurately measure voltage and amperage.

The traversing mechanism enabled three-dimensional movement of the thermocouple and hot-film anemometer probes. This device was capable of accurate measurements to less than 2.54×10^{-5} m. It was constructed of three mutually orthogonal "Unislides". Scales were added so that readings in 2.54×10^{-5} m could be noted directly. The traversing mechanism was secured to a 0.0762 m thick by 0.6096 m long aluminum bed which was bolted to the top edge of the plexiglas tank, thereby yielding a stable configuration. Specific adapter rods were designed to best handle the particular probe in question.

The thermocouple probe was constructed of 5.08×10^{-5} m copper–constantan wire. It is shown in [1]. The probe was calibrated over a range of 293.15–333.15 K with six points using a difference curve calibration [4].

The hot-film anemometry equipment was procured from Thermo-Systems, Inc., St. Paul, Minnesota. It is a constant-temperature hot-film anemometer and designated as a 1010A unit by Thermo-Systems, Inc. The probes used in this investigation were hot-film types, quartz-coated in order to be usable in a conducting fluid such as water. The probe used in the velocity measurement determinations was a 1212-10W, i.e. a probe with a 2.54×10^{-5} m quartz-coated hot-film sensor.

Calibration of the probe over ranges of temperature and velocity was effected by means of two-tanks especially constructed for this purpose. Two were built: for horizontal and vertical tows. Essentially, they consisted of a probe-holder block which could run on rails by being dragged through the solution. The tanks had a traverse of about 0.381 m which is suitable for low velocity measurements. The power for towing was supplied by the chart drive of a recorder by means of a gearing arrangement designed for the purpose. The tanks were insulated and had a capacity of about 7.5708×10^{-3} m^3.

Physical property measurements

Since polymer solutions have properties which vary with both preparation, aging and type, it was necessary to measure all pertinent physical property data for the solutions used in these experiments. The data required were for density, coefficient of thermal expansion, thermal conductivity, and rheological properties. Also, the physical property data had to be obtained as a function of temperature to be used in this work.

The works reported in this paper used two different polymers, each at two different concentrations. The polymers used in this study were CMC-7H (Hercules—Carboxymethylcellulose) and Polyox WSR-FRA [Union Carbide—poly (ethylene) oxide]. The concentrations used were 0.5% CMC-7H and 1% CMC-7H; and 0.25% Polyox WSR-FRA and 0.5% Polyox WSR-FRA. Solution preparation was done with a minimum of shearing and by using distilled water which avoided bubble formations during the heat-transfer runs and also stayed fresher longer. The solutions were made up in 0.3785 m^3 batches. The CMC-7H was prepared by slowly stirring in the polymer to the mixing tank so that it was dispersed, but also fast enough so that the solution viscosity did not yet have time to change. The stirring was continued for 8.64×10^4 s at a slow rate in order to effect solution. The polyox solutions were more difficult to work with. It is almost impossible to dissolve the polyox quickly and evenly without the aid of a dispersing agent, i.e. a fluid which wets the polymer without dissolving it so that it can be quickly dispersed into the water and each particle solvated. The dispersing agent used in this preparation was isopropyl alcohol. It mixes well with water and is relatively inert with respect to equipment. It was used in the ratio of 3 parts of alcohol to each part of polymer. Trace amounts of copper sulfate were added to all solutions to prevent biological growth.

The measurement of properties was done simultaneously with the running of the heat-transfer experiments so that exact property values could be evaluated for the particular solution.

Density measurement

The density of any polymer solution at any temperature was obtained by using a calibrated Thomas pycnometer in conjunction with a constant temperature bath accurate to 0.05 K. The meniscus of the fluid in the pycnometer was measured using a cathetometer. The density vs temperature relationship for each solution was fitted by least-squares techniques to a quadratic polynomial. This data is listed in Table 1 for a range of 293.15 to 333.15 K.

Coefficient of thermal expansion

The coefficient of thermal expansion, β, can be computed from the density formula through the use of the defining equation:

$$\beta = \frac{1}{\rho}\left(\frac{\partial \rho}{\partial T}\right)_p. \tag{20}$$

Table 1. Density–temperature polynomial coefficient for polymer solutions
$\rho = [a + b(T-273.15) + C(T-273.15)^2]10^3$
ρ = kg/m^3 T = K $293.15 \leqslant T \leqslant 333.15$ K

Solution	Constant a	Constant b	Constant c
0.5% CMC-7H	1.0045	$-1.7396(10^{-4})$	$-2.3897(10^{-6})$
1.0% CMC-7H	1.0050	$-5.8154(10^{-5})$	$-3.7971(10^{-6})$
0.25% Polyox WSR-FRA	0.9939	$-9.6665(10^{-5})$	$-3.3115(10^{-6})$
0.50% Polyox WSR-FRA	0.99997	$-1.5559(10^{-4})$	$-2.7478(10^{-6})$

Thermal conductivity measurements

The thermal conductivity vs temperature for each polymer solution was measured through the use of a concentric-cylinder thermal conductivity cell designed by the authors and described fully in [3]. This cell could measure thermal conductivity to within $\pm 2\%$.

Table 2. Thermal conductivity–temperature polynomial coefficients for polymer solutions
$k = 4{\cdot}1868 \times 10^2[a+b(T-273.15)]$
k = J/m·s·K, T = K, $298.15 \leqslant T \leqslant 323.15$ K

Solution	Constant a	Constant b
0.5% CMC-7H	$1.251(10^{-3})$	$6.626(10^{-6})$
1.0% CMC-7H	$1.194(10^{-3})$	$9.906(10^{-6})$
0.25% Polyox WSR-FRA 0.50% Polyox WSR-FRA	$1.121(10^{-3})$	$9.323(10^{-6})$

The results of the thermal conductivity measurements are shown in Table 2. Note that the polyox solutions are fitted by one equation, a result probably due to the effect of the isopropyl alcohol. The equations for thermal conductivity vs temperature are linear.

Heat capacity data

The heat capacity of the polymer solution was assumed to be the same as for water, viz. $c_p = 4.1868 \times 10^3$ J/kg K.

Rheological data for polymer solutions

The flow curves for all polymer solutions were obtained through the use of an R-16 Weissenberg Rheogoniometer equipped with temperature control. Measurements were made with a 0.01745 rad–0.1 m cone and plate in both steady rotational shear and steady rotational normal force. The normal force work confirmed the fact that the polyox solutions were viscoelastic while the CMC solutions were not. Both types of solutions were evaluated in terms of the power law parameters over a wide range of temperatures: 298.15, 303.15 and 308.15 K. It was not feasible to get good data above these temperatures since the fluid started to evaporate, causing film formation at the outer edge of the cone and plate inducing an added and unknown drag on the upper platen.

It should be noted that the solutions showed little dependency of n, the flow parameter index, on temperature, so that for any fluid, only one value is given. Also, the 0.5% Polyox WSR-FRA exhibited two regions of behavior depending on shear rate, and thus, two values of n. The low shear rate value was chosen since free convection usually involves low shear rates. The summary of rheological data is shown in Table 3.

EXPERIMENTAL PROCEDURE

An experimental heat-transfer run consisted in placing the sphere supported by the support tube in a rigid assembly, into the center of the tank. Power was then turned on and a steady-state was attained as noted by the e.m.f. measurements of the sphere thermocouples by the potentiometer. Steady-state was assumed when the e.m.f. reading differed by less than 2μV over a 900 s period. The tank bulk temperature was measured with a thermometer and a thermocouple at different positions. They agreed closely with each other. Another run was obtained by increasing the voltage. This procedure continued until the power level for the particular sphere would be excessive under the operating conditions. This was done for each polymer solution.

The temperature and velocity profile measurements required much initial calibration work. The temperature probe was calibrated, as stated above and was considered to be accurate to better than 0.1 K. Temperature profiles were measured in 0.25% Polyox WSR-FRA, 0.50% Polyox WSR-FRA and 0.50% CMC-7H. The temperature coefficient of resistance of the hot-

Table 3. Rheological data for polymer solutions

CMC–solution
$K = A\exp(B/T)$
$K = \text{N s}^n/\text{m}^2$, T = K, $298.15 \leqslant T \leqslant 308.15$ K

Solution	Constant A	Constant B	n
0.5% CMC-7H	$5.65(10^{-6})$	2895	0.948*
1.0% CMC-7H	$5.13(10^{-7})$	4250	0.818†

*$0.173\,\text{s}^{-1} \leqslant \gamma \leqslant 274\,\text{s}^{-1}$
†$0.173\,\text{s}^{-1} \leqslant \gamma \leqslant 274\,\text{s}^{-1}$

Polyox solutions
$K = A+B(T-273.15)$
$K = \text{N s}^n/\text{m}^2$, T = K, $298.15 \leqslant T \leqslant 308.15$ K

Solution	Constant A	Constant B	n
0.25% Polyox WSR-FRA	0.292	−0.00451	0.592‡
0.50% Polyox WSR-FRA	6.08	−0.127	0.905§

‡$0.173\,\text{s}^{-1} \leqslant \gamma \leqslant 274\,\text{s}^{-1}$
§$0.00345\,\text{s}^{-1} \leqslant \gamma \leqslant 0.274\,\text{s}^{-1}$.

film probe was determined by cold resistance measurements in a constant temperature bath. With this information, one could then select a sensor operating temperature from the overheat ratio. Two overheat ratios were chosen: 1.05 and 1.10, but only 1.10 was used. There must be a choice between response and bubble formation on the probe, that is to say, that a high overheat ratio gives better response and sensitivity, but two, at each overheat ratio. The tank temperatures used with the 1.10 overheat ratio were 296.45, 301.35, 305.85, 311.45, 317.05, 320.85 and 324.55 K. The velocity ranged from 3×10^{-4} m/s to 0.14 m/s. Calibration curve in 0.5% CMC-7H is shown in Fig. 1(b). Also presented is the calibration curve for water in order to show the non-Newtonian effect on anemometry (see Fig. 1a).

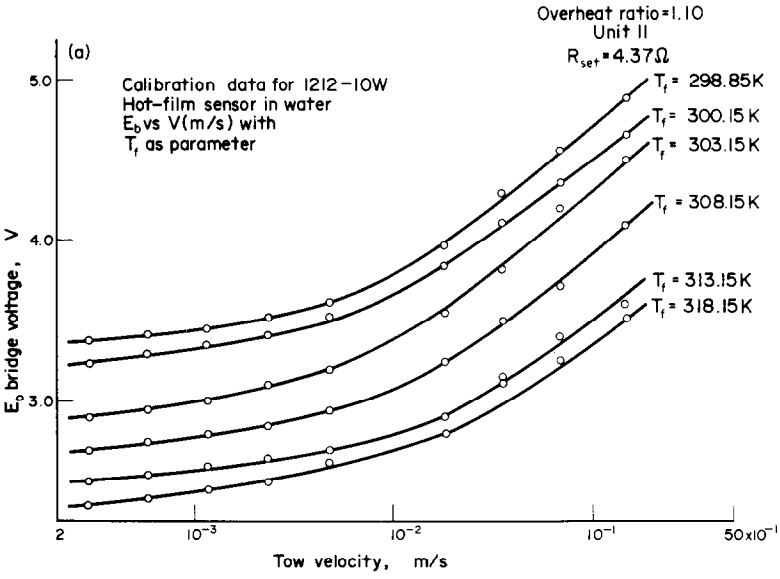

FIG. 1(a). Calibration curve of hot film sensor (water).

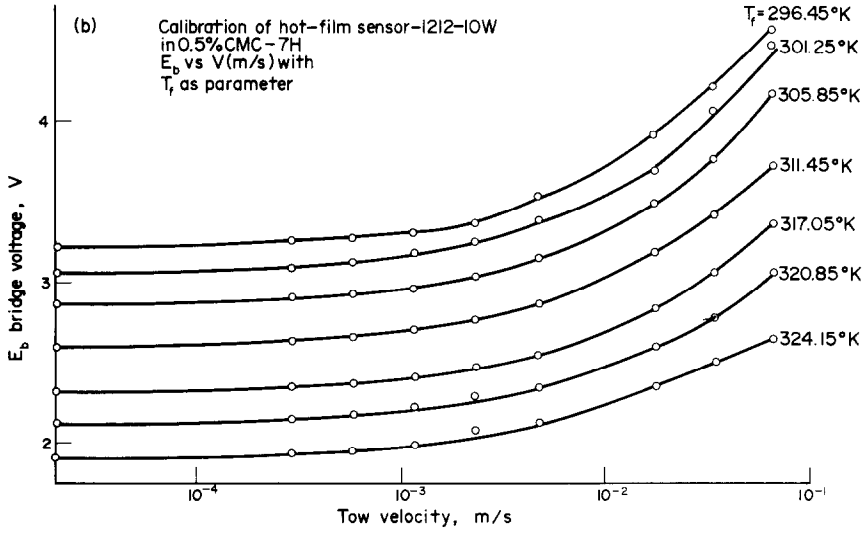

FIG. 1(b). Calibration curve of hot film sensor (CMC solution).

it also means a higher temperature which is bounded by the boiling point of the liquid and even more so by the evolution of air bubbles on the sensor. Thus, fresh distilled water was a must in solution preparation. Also, velocity measurements were only obtained in the 0.5% CMC-7H solution. Next, a double calibration was performed by measuring the bridge voltage response at a given temperature for varying velocities of

With the hot-film probe fully calibrated, one next proceeds to measure the temperature field at some position normal to the surface of the sphere using the traversing mechanism in conjunction with a cathetometer. Conduction effects along the thermocouple probe were investigated using previously developed analyses [5, 6]. The velocity field at this same position is measured with the hot-film probe, again using the

traversing mechanism. We now have bridge voltage and temperature data as a function of distance. Therefore, we can now use the double calibration curves to find the velocities which correspond to the particular distance measurements. Thus, we can fully delineate the velocity profile. The measurements of temperature and velocity fields were confined to the 3-in sphere alone and the measurements normal to the sphere surface were taken at the stagnation point, the $\pi/4$ rad position, $\pi/2$ rad position, and $3/4\pi$ rad position. A horizontal traverse was taken at the top of the sphere, i.e. cutting across the plume.

Also, if n is set equal to unity in equation (23), then the value of the constant, viz. 0.489 determined experimentally, corresponds very closely with the value predicted by Acrivos for the large Prandtl number analysis, viz. 0.49.

Temperature profile measurements in polymer solutions

Figures 3–6 show typical temperature profiles obtained in the 0.5% CMC-7H and the 0.25% Polyox WSR-FRA for the 0.0762 m sphere at 112 W power input. Much more extensive profile measurements are available in [3] for the 0.50% CMC-7H and 0.25%

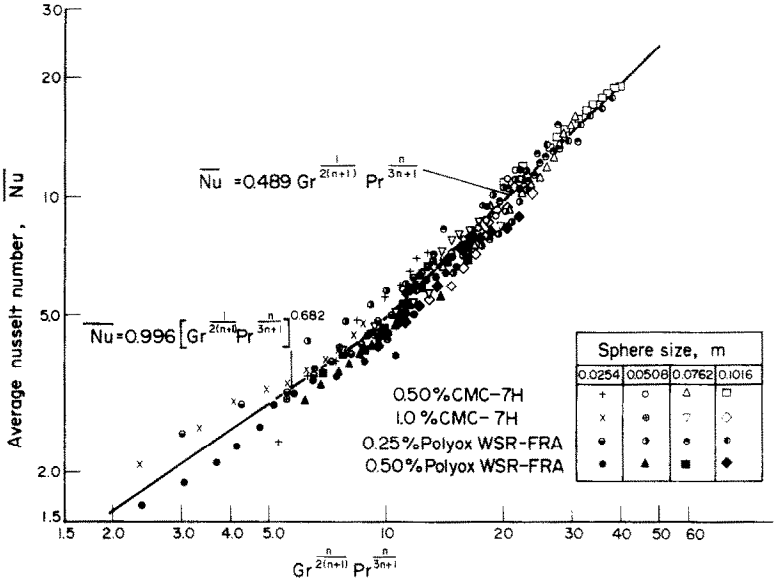

FIG. 2. Correlation of free convection heat transfer from isothermal spheres in polymer solutions.

RESULTS AND DISCUSSION

The results of free convection heat transfer from spheres in the polymer solutions described here is shown in Fig. 2. The data for all solutions has been correlated according to equation (17). An interesting result is visible from Fig. 2. We see that for

$$Z \equiv Gr^{1/[2(n+1)]}Pr^{n/(3n+1)} < 10 \qquad (21)$$

we have a region of differing heat transfer. In particular, for $Z < 10$, the average Nusselt number may be represented by

$$\overline{Nu} = C_1 Z^D \qquad (22)$$

where $C_1 = 0.996 \pm 0.120$ and $D = 0.682 \pm 0.062$ and with a mean error of 8% for $1.5 < \overline{Nu} \leqslant 5.0$.

For the region, $Z > 10$, the heat-transfer results can be represented by the following average Nusselt number:

$$\overline{Nu} = C_2 Z \qquad (23)$$

where $C_2 = 0.489 \pm 0.005$ and with a mean error of 7.6% for $5 < \overline{Nu} \leqslant 20$ and $10 < Z \leqslant 40$. These results correspond nicely to Acrivos' [2] prediction that an equation of the form of (23) would be valid for $Z > 10$.

Polyox WSR-FRA at 28 and 56 W and for the 0.50% Polyox WSR-FRA at 28 and 56 W.

The temperature profile measurements were taken at the bottom stagnation point, $\pi/4$ rad, $\pi/2$ rad, $3/4\pi$ rad position and also at the horizontal traverse across the plume at the π rad position. At this top-most position, one can observe the formation of a "bell-shaped" profile which is characteristic of plumes.

Figure 7 shows the plot of data for both water and 0.50% CMC-7H on a θ vs η graph. The line represents the result of extending Acrivos' [2] work to generate the full profile (within the boundary layer). The agreement is seen to be quite good.

Local heat transfer from a sphere in polymer solutions

Figures 8 and 9 show the local heat-transfer variation on a sphere as a function of angular distance from the stagnation point compared with Acrivos' [2] theory.

In order to calculate the local values of heat transfer, it was necessary to least squares fit the profile data at 0 rad, $\pi/4$ rad, $\pi/2$ rad and $3/4\pi$ rad in order to obtain accurate and consistent values of $-\theta'(0)$. The first ten points of the profile were fit to a linear equation

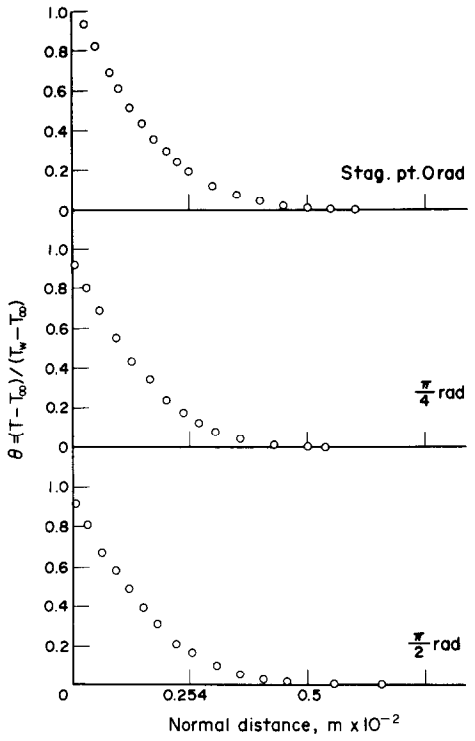

FIG. 3. Temperature profiles, θ vs y, 0.0762 m sphere—112 W, 0.5% CMC-7H; 0 rad, $\pi/4$ rad, and $\pi/2$ rad positions.

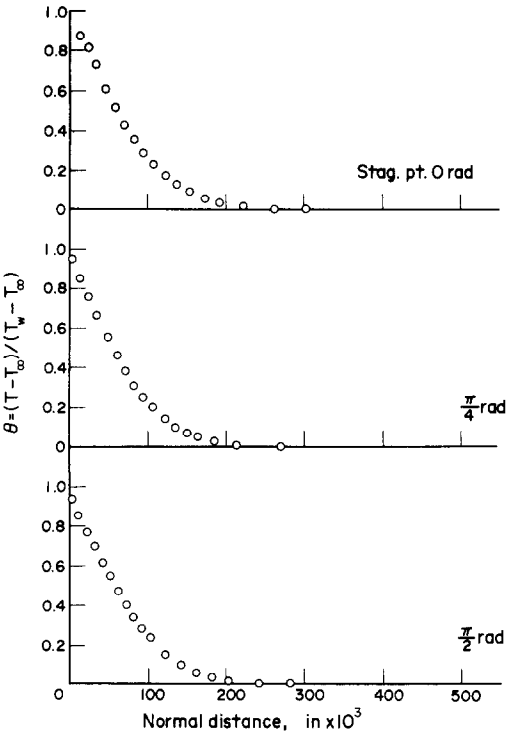

FIG. 5. Temperature profiles, θ vs y, 0.0762 m sphere—112 W, 0.25% Polyox WSR-FRA; 0 rad, $\pi/4$ rad, and $\pi/2$ rad positions.

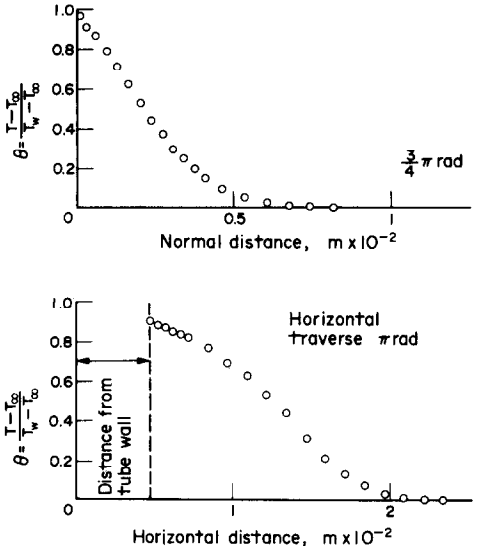

FIG. 4. Temperature profiles, θ vs y, 0.0762 m sphere—112 W, 0.5% CMC-7H; $3/4\pi$ rad and horizontal traverse (π rad) positions.

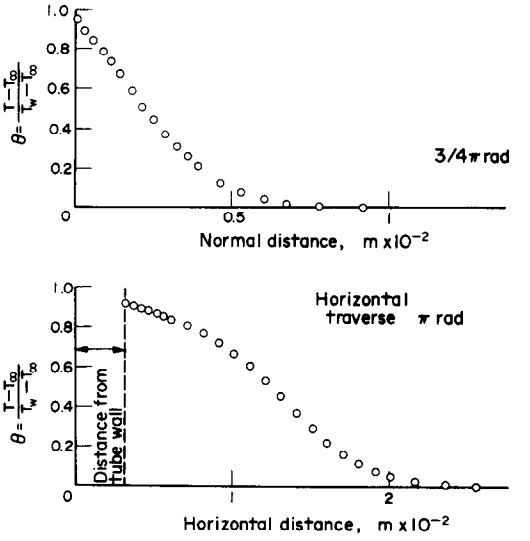

FIG. 6. Temperature profiles, θ vs y, 0.0762 m sphere—112 W, 0.25% Polyox WSR-FRA; $3/4\pi$ rad and horizontal traverse (π rad) positions.

according to the following rationale: If the energy equation for heat transfer by fee convection is evaluated at the wall, it is immediately true that $\partial^2\theta/\partial y^2|_{y=0}$ equals zero. If the temperature function is expanded in a Taylor series about the point $y = 0$, then it is seen that the use of a linear equation is already accurate to terms of $O(y^3)$. An even better fit would be achieved by using a cubic without the quadratic term, but the additional refinement is probably not warranted.

The following conclusions can be drawn from the local heat-transfer data: (a) the heat transfer at the stagnation point is the highest of any point on the sphere, and (b) the heat transfer falls off very slowly in the first $\pi/2$ rad, after which it decreases quite rapidly. Almost two-thirds of the total heat transfer occurs on the bottom half of the sphere.

Thermal boundary-layer thicknesses

Figures 10 and 11 show plots of a dimensionless boundary-layer thickness vs dimensionless distance

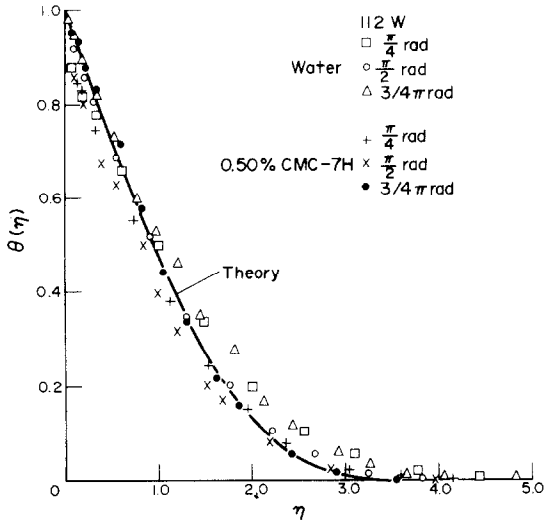

FIG. 7. Dimensionless temperature profile: θ vs η.

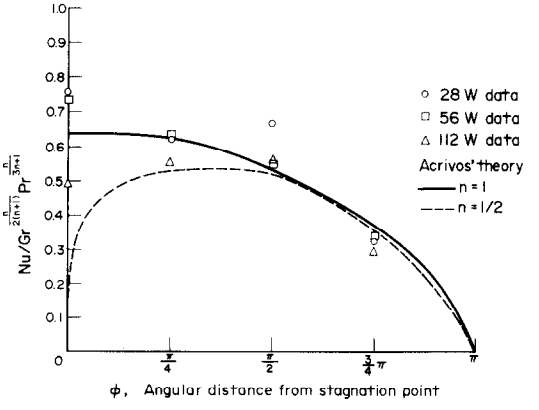

FIG. 8. Variation in local heat-transfer rate along sphere in 0.5% CMC-7H, based on radius, ($n = 0.948$).

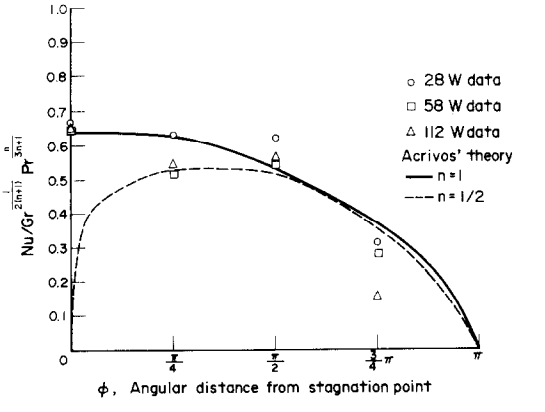

FIG. 9. Variation in local heat-transfer rate along sphere in 0.25% Polyox WSR-FRA, based on radius, ($n = 0.592$).

from the stagnation point for 0.5% CMC-7H and 0.25% Polyox WSR-FRA, respectively. The "scaling factor" is the generalized Rayleigh number (average) based on the radius of the sphere.

A general trend can be seen, viz. that the boundary layer is quite thick at the stagnation point, then begins to thin as it moves to the $\pi/4$ rad and $\pi/2$ rad positions,

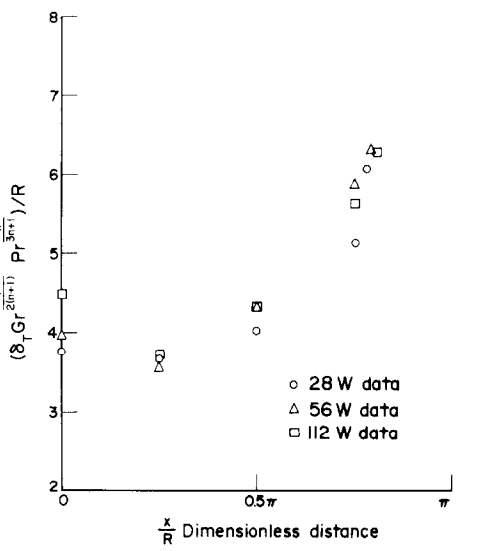

FIG. 10. Dimensionless thermal boundary-layer thickness vs dimensionless distance from stagnation point for 0.5% CMC-7H.

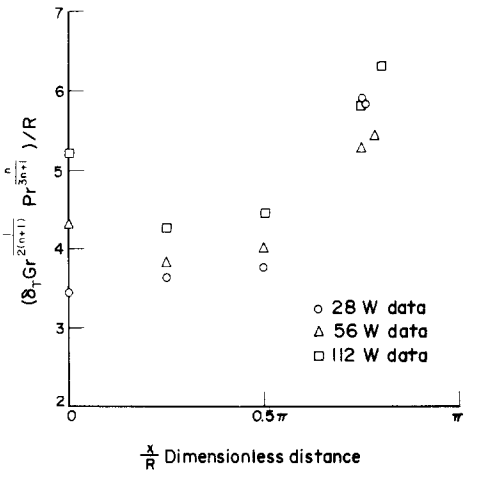

FIG. 11. Dimensionless thermal boundary-layer thickness vs dimensionless distance from stagnation point for 0.25% Polyox WSR-FRA.

and finally thickens as it moves into the plume region. It can also be seen that the thermal boundary-layer thickness is thicker in the 0.5% CMC-7H when compared to water at the same power input, as shown in Table 5. Further data can be found in [3].

Velocity profile measurements

Figures 12–15 show the results of measuring velocity profiles in 0.5% CMC-7H at 112 W input for the 0.0762 m sphere. An interesting result is to be noted for this polymer solution in that the velocity rises quickly to a maximum and then falls off rapidly to a lower value, after which it tapers off very slowly, thereby giving a very thick layer. The $\pi/4$ rad and $\pi/2$ rad data do not have a defined maximum due to the failure to start the traverse close enough to the wall. The maximums can be estimated for these traverses and together with the $3/4\pi$ rad and π rad traverses are listed

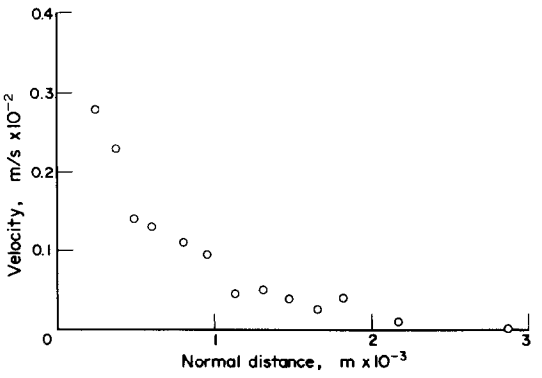

FIG. 12. Velocity profile in 0.5% CMC-7H, 0.0762 m sphere, 112 W, $\pi/4$ rad position.

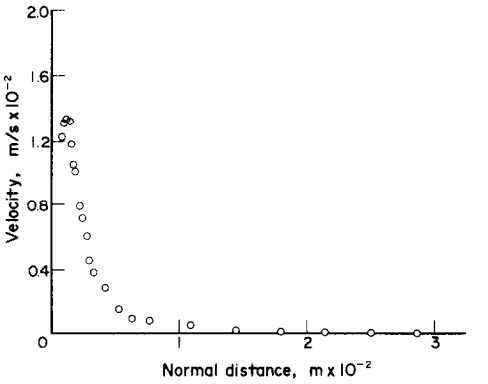

FIG. 14. Velocity profile in 0.5% CMC-7H, 0.0762 m sphere, 112 W, $3/4\pi$ rad position.

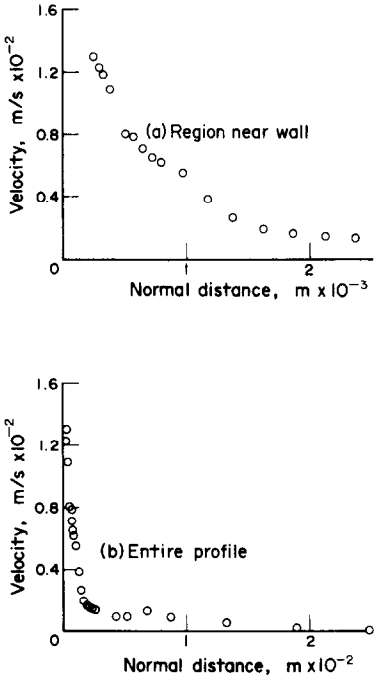

FIG. 13. Velocity profile in 0.5% CMC-7H, 0.0762 m sphere, 112 W, $\pi/2$ rad position.

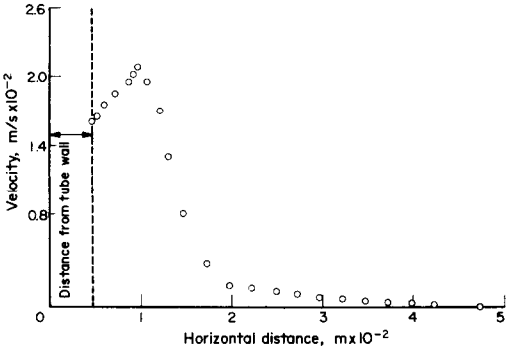

FIG. 15. Velocity profile in 0.5% CMC-7H, 0.0762 m sphere, 112 W, horizontal traverse—π rad.

Table 4. Maximum velocities in free convection flow about a sphere in 0.5% CMC-7H as a function of angular distance from the stagnation point

rad	Maximum velocity (m/s)
$\pi/4$	0.29×10^{-2}
$\pi/2$	1.30×10^{-2}
$3/4\pi$	1.40×10^{-2}
π (Horizontal traverse)	2.10×10^{-2}

in Table 4. Another point of interest is that the maximums obtained in the 0.5% CMC-7H solution are not markedly different from those obtained in water as shown in [1].

Velocity boundary-layer thicknesses

Table 5 shows the data for the velocity boundary-layer thicknesses for the 3 in sphere in a 0.5% CMC-7H solution at 112 W input. As to be expected, the velocity

Table 5. Comparison of temperature and velocity boundary-layer thicknesses and their ratio in water and in 0.5% CMC-7H for positions around a sphere (0.0762 m sphere—112 W)

	Position	$\delta_T m$	$\delta_v m$	δ_T/δ_v
Water	$\pi/4$	2.743×10^{-3}	3.556×10^{-3}	0.772
	$\pi/2$	2.769×10^{-3}	7.366×10^{-3}	0.376
	$3/4\pi$	4.420×10^{-3}	1.371×10^{-3}	0.322
	π	2.545×10^{-2}	2.997×10^{-3}	0.849
0.5% CMC-7H	$\pi/4$	7.239×10^{-3}	2.921×10^{-3}	2.48
	$\pi/2$	7.925×10^{-3}	2.286×10^{-3}	0.346
	$3/4\pi$	1.011×10^{-2}	2.901×10^{-2}	0.348
	π	3.363×10^{-2}	4.826×10^{-2}	0.697

boundary-layer thickness in 0.5% CMC-7H is much thicker, overall than that in water. In Table 5 is also shown the ratio of thermal to velocity boundary-layer thicknesses for both water and 0.5% CMC-7H. The main conclusion here is that (except at the stagnation point) the ratios δ_T/δ_v in both water and 0.5% CMC-7H are essentially the same.

CONCLUSIONS

The heat transfer by natural convection from spheres in widely differing (non-Newtonian viscous and non-Newtonian viscoelastic) polymer solutions has been shown to follow the power-law theory of Acrivos [2] for a value of

$$Z \equiv Gr^{1/[2(n+1)]}Pr^{n/(3n+1)} > 10$$

by the following expression:

$$\overline{Nu} = C_2 Z$$

where $C_2 = 0.489 \pm 0.005$ with a mean error of 7.6% for $10 < Z \leqslant 40$ and $5 < \overline{Nu} \leqslant 20$.

For $Z < 10$, the following correlation applies:

$$\overline{Nu} = C_1 Z^D$$

where $C_1 = 0.996 \pm 0.120$ and $D = 0.682 \pm 0.062$ with a mean error of 8% for $1.5 < \overline{Nu} \leqslant 5.0$.

Quantitative data have been obtained in polymer solutions on the temperature and velocity profiles, local heat transfer from a sphere, thermal boundary-layer thicknesses, velocity boundary-layer thicknesses and their ratios, for the case of a sphere in free convection. Hot-film anemometry has been extended from the case of velocity measurement in a non-isothermal, free convection system (water) as shown in [1, 3], to the case of velocity measurement in a non-isothermal, free convection system (polymer solution).

Acknowledgements—The authors wish to thank the National Science Foundation for its financial support, in part, through Grant No. GK-408.

REFERENCES

1. W. S. Amato and Chi Tien, Free convection heat transfer from isothermal spheres in polymer solutions, *Int. J. Heat Mass Transfer* **15**, 327–339 (1972).
2. A. Acrivos, A theoretical analysis of laminar free convection heat transfer to non-Newtonian fluids, *A.I.Ch.E. Jl* **6**, 584–590 (1960).
3. W. S. Amato, Free convection heat transfer in water and polymer solutions, Ph.D. Dissertation, Syracuse University, Syracuse, New York (1970).
4. W. F. Roeser and H. T. Wensel, *Temperature: Its Measurement and Control in Science and Industry*, pp. 284–313, American Institute of Physics, Reinhold, New York (1941).
5. M. Jakob, The influence of the free end of a rod on heat transfer, *Phil. Mag.* **28**, 571–578 (1939).
6. E. F. C. Somerscales, Experimental investigation of the temperature distribution in a horizontal fluid layer heated from below, Ph.D. Dissertation, Cornell University, Ithaca, New York (1965).

TRANSFERT DE CHALEUR PAR CONVECTION NATURELLE AUTOUR DE SPHERES ISOTHERMES DANS DES SOLUTIONS DE POLYMERES

Résumé—On présente une étude expérimentale du transfert de chaleur par convection naturelle autour de sphères isothermes dans des solutions aqueuses de polymères. Les données sont corrélées à l'aide d'un modèle en loi puissance suivant la théorie de Acrivos [2]. Les profils de température ont été mesurés autour d'une sphère isotherme dans diverses solutions de polymères et les profils de vitesse autour de la sphère en convection naturelle ont été obtenus à l'aide d'un anémomètre à fil chaud dans une solution de polymère. Des renseignements quantitatifs sur les épaisseurs de couche limite sont également obtenus.

WÄRMEÜBERGANG BEI FREIER KONVEKTION VON ISOTHERMEN KUGELN IN POLYMER-LÖSUNGEN

Zusammenfassung—Es wird über eine experimentelle Untersuchung des Wärmeübergangs bei freier Konvektion von isothermen Kugeln an wäßrige Polymer-Lösungen berichtet. Nach der Theorie von Acrivos wurde ein Potenzgesetz zur Korrelation der Ergebnisse herangezogen. Temperaturprofile um eine isotherme Kugel wurden in verschiedenen Polymer-Lösungen gemessen; nach der Heiß-Film-Anemometrie ließen sich Geschwindigkeitsprofile um eine Kugel bei freier Konvektion in einer Polymer-Lösung bestimmen. Es wurden auch quantitative Ergebnisse für die Grenzschichtdicken erhalten.

СВОБОДНО-КОНВЕКТИВНЫЙ ТЕПЛООБМЕН МЕЖДУ ИЗОТЕРМИЧЕСКИМИ СФЕРАМИ И ПОЛИМЕРНЫМИ РАСТВОРАМИ

Аннотация — Проведено экспериментальное исследование свободно-конвективного теплообмена между изотермическими сферами и водными полимерными растворами. Модель степенной жидкости использовалась для обобщения данных согласно теории Акривоса [2]. Измерялись температурные профили вблизи изотермической сферы в различных полимерных растворах. Профили скорости вблизи поверхности сферы в полимерном растворе измерялись с помощью термоанемометра с нагреваемой пленкой. Получены также количественные оценки толщины пограничного слоя.